Structures and Sorption Properties of Ionic Crystals of Macrocation-Dawson-Type Polyoxometalates with Different Charges

Sayaka Uchida, Ryosuke Kawamoto, Takeo Akatsuka, Shiro Hikichi, and Noritaka Mizuno*

Department of Applied Chemistry, School of Engineering, The University of Tokyo, 7-3-1 Hongo, Bunkyo-ku, Tokyo 113-8656, Japan

Received December 6, 2004. Revised Manuscript Received January 11, 2005

The complexation of Dawson-type polyoxometalates of $[\alpha\text{-}P_2W_{18}O_{62}]^{6-}$, $[\alpha_2\text{-}P_2W_{17}V_1O_{62}]^{7-}$, and $[\alpha\text{-}P_2W_{15}V_3O_{62}]^{9-}$ with the macrocation ($[Cr_3O(OOCH)_6(H_2O)_3]^+$) forms ionic crystals of $(NH_4)_4[Cr_3O(OOCH)_6(H_2O)_3]_2[\alpha\text{-}P_2W_{18}O_{62}]\cdot 15H_2O$ (**1a**), $(NH_4)_5[Cr_3O(OOCH)_6(H_2O)_3]_2[\alpha_2\text{-}P_2W_{17}V_1O_{62}]\cdot 15H_2O$ (**2a**), and $(NH_4)_7[Cr_3O(OOCH)_6(H_2O)_3]_2[\alpha\text{-}P_2W_{15}V_3O_{62}]\cdot 15H_2O$ (**3a**), respectively. The compounds **1a**−**3a** show the honeycomb packing and the symmetry of the constituent ions reflect on the crystal structures. The lengths of the *a* axes of **1a**−**3a** are almost the same, while those of the *c* axes decrease in the order of **1a** ≥ **2a** > **3a**, with the increase in the anion charges of the polyoxometalates. The water of crystallization in **1a**−**3a** is desorbed by the evacuation at 373 K to form the respective guest-free phases **1b**−**3b**. The compounds **1b**−**3b** are crystalline, and the lengths of the *a* axes of **1b**−**3b** are almost the same, while those of the *c* axes decrease in the order of **1b** ≥ **2b** > **3b**. The compounds **1b**−**3b** possess voids running perpendicular to the *c* axis. The sizes of the voids decrease in the order of **1b** > **2b** > **3b** and are comparable to those of water and methanol. The water sorption profile of **1b** as a function of time is reproduced by the linear driving force mass transfer model with a single rate constant k_1, while that of **3b** is reproduced by the two components k_1 and k_2. The component k_1 is attributed to the diffusion of water molecules in the voids, and the component k_2 is attributed to the large increase in the length of the *c* axis with the water sorption. The compounds **1b** and **2b** sorb ethanol, while the amount of sorption for **2b** is smaller than that for **1b**, and **3b** completely excludes ethanol. Thus, the crystal structures, water sorption kinetics, and alcohol sorption properties of **1b**−**3b** systematically change with the anion charges.

Introduction

There are considerable interests in the construction of either inorganic zeolites[1] or inorganic/organic hybrid nanostructured compounds.[2] The inorganic/organic hybrid nanostructures give rise to the unique selectivity in the guest sorption,[3] ion exchange,[4] and catalysis.[5] The rational design of nanostructured compounds by the use of molecular building blocks has been recently developed. The geometry of the frameworks of the compounds can be predicted from the shapes, sizes, and functional groups of the inorganic and organic building blocks, which assemble with the coordination bonds[2a,2f] and hydrogen bonds.[2b] For example, inorganic building blocks with tetrahedral and triangular metal centers give the diamond and hexagonal frameworks, respectively.[2a] Such rational design has not yet been addressed in the syntheses of ionic crystals.

Polyoxometalates are nanosized discrete metal−oxygen cluster anions and attractive building blocks of nanostructured ionic crystals.[6] Polyoxometalates show unique redox or acidic properties, which can be controlled by the changes of the constituent elements, configuration, sizes, charges, etc. These properties have extensively been applied in the fields of catalysis.[7] The complexation of Keggin-type $[\alpha\text{-}SiW_{12}O_{40}]^{4-}$ and $[\alpha\text{-}CoW_{12}O_{40}]^{6-}$ polyoxometalates (T_d) with the macrocation $[Cr_3O(OOCH)_6(H_2O)_3]^+$ (D_{3h}) formed ionic crystals of $K_3[Cr_3O(OOCH)_6(H_2O)_3][\alpha\text{-}SiW_{12}O_{40}]\cdot 16H_2O$[8] (mono-

(1) (a) Corma, A. *Chem. Rev.* **1995**, *95*, 559. (b) van Santen, R. A.; Kramer, G. J. *Chem. Rev.* **1995**, *95*, 637. (c) Thomas, J. M. *Angew. Chem. Int. Ed.* **1999**, *38*, 3588. (d) Wight, A. P.; Davis, M. E. *Chem. Rev.* **2002**, *102*, 3589. (e) Tsapatsis, M. *AIchE J.* **2002**, *48*, 654. (f) Davis, M. E. *Nature* **2002**, *417*, 813. (g) Serre, C.; Taulelle, F.; Férey, G. *Chem. Commun.* **2003**, 2755.

(2) (a) Eddaoudi, M.; Moler, D. B.; Li, H.; Chen, B.; Reineke, T. M.; O'Keeffe, M.; Yaghi, O. M. *Acc. Chem. Res.* **2001**, *34*, 319. (b) Moulton, B.; Zaworotko, M. J. *Chem. Rev.* **2001**, *101*, 1629. (c) Férey, G. *Chem. Mater.* **2001**, *13*, 3084. (d) Evans, O. R.; Lin, W. *Acc. Chem. Res.* **2002**, *35*, 511. (e) Yaghi, O. M.; O'Keeffe, M.; Ockwig, N. W.; Chae, H. K.; Eddaoudi, M.; Kim, J. *Nature* **2003**, *423*, 705. (f) Kitagawa, S.; Kitaura, R.; Noro, S. *Angew. Chem. Int. Ed.* **2004**, *43*, 2334.

(3) (a) Albrecht, M.; Lutz, M.; Spek, A. L.; van Koten, G. *Nature* **2000**, *406*, 970. (b) Edgar, M.; Mitchell, R.; Slawin, M. Z.; Lightfoot, P.; Wright, P. A. *Chem.−Eur. J.* **2001**, *7*, 5168. (c) Cussen, E. J.; Claridge, J. B.; Rosseinsky, M. J., Kepert, C. J. *J. Am. Chem. Soc.* **2002**, *124*, 9574. (d) Kosal, M. E.; Chou, J. H.; Wilson, S. R.; Suslick, K. S. *Nature Mater.* **2002**, *1*, 118. (e) Rosi, N. L.; Eckert, J.; Eddaoudi, M.; Vodak, D. T.; Kim, J.; O'Keefee, M.; Yaghi, O. M. *Science* **2003**, *300*, 1127. (f) Pan, L.; Adams, K. M.; Hernandez, H. E.; Wang, X.; Zheng, C.; Hattori, Y.; Kaneko, K. *J. Am. Chem. Soc.* **2003**, *125*, 3062. (g) Dybtsev, D. N., Chun, H.; Yoon, S. H.; Kim, D.; Kim, K. *J. Am. Chem. Soc.* **2004**, *126*, 32.

(4) (a) Yaghi, O. M.; Li, H. *J. Am. Chem. Soc.* **1996**, *118*, 295. (b) Yaghi, O. M.; Li, H.; Groy, T. L. *Inorg. Chem.* **1997**, *36*, 4292. (c) Darlrymple, S. A.; Shimizu, G. K. H. *Chem.−Eur. J.* **2002**, *8*, 3010.

(5) (a) Fujita, M.; Kwon, Y. J.; Washizu, S.; Ogura, K. *J. Am. Chem. Soc.* **1994**, *116*, 1151. (b) Seo, J. S.; Whang, D.; Lee, H.; Jun, S. I.; Oh, J.; Jeon, Y. J.; Kim, K. *Nature* **2000**, *404*, 982. (c) Naito, S.; Tanibe, T.; Saito, E.; Miyao, T. Mori, W. *Chem. Lett.* **2001**, 1178. (d) Dewa, T.; Saiki, T.; Aoyama, Y. *J. Am. Chem. Soc.* **2001**, *123*, 502. (e) Gomez-Lor, B.; Gutiérrez-Puebla, E.; Iglesias, M.; Monge, M. A.; Ruiz-Valero, C.; Snejko, N. *Inorg. Chem.* **2002**, *41*, 2429. (f) Pan, L.; Liu, H.; Lei, X.; Huang, X.; Olson, D. H., Turro, N. J.; Li, J. *Angew. Chem. Int. Ed.* **2003**, *42*, 542.

10.1021/cm047879s CCC: $30.25
Published on Web 02/18/2005

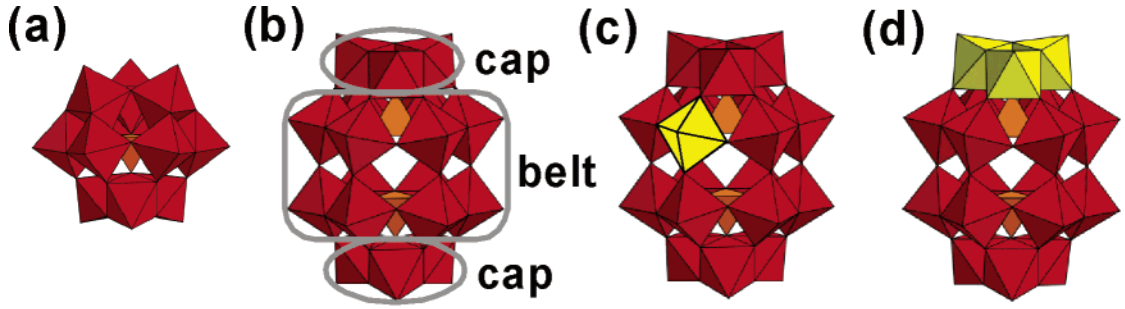

Figure 1. Molecular structures of the Keggin- and Dawson-type polyoxometalates. (a) Keggin-type $[\alpha\text{-}PW_{12}O_{40}]^{3-}$, (b) Dawson-type $[\alpha\text{-}P_2W_{18}O_{62}]^{6-}$, (c) Dawson-type $[\alpha_2\text{-}P_2W_{17}V_1O_{62}]^{7-}$, and (d) Dawson-type $[\alpha\text{-}P_2W_{15}V_3O_{62}]^{9-}$. Red, yellow, and orange polyhedra showed the $[WO_6]$, $[VO_6]$, and $[PO_4]$ units, respectively.

clinic, *C*2/*m*) and $Cs_5[Cr_3O(OOCH)_6(H_2O)_3][\alpha\text{-}CoW_{12}O_{40}]\cdot 7.5H_2O$[9] (monoclinic, $P2_1/c$), respectively. The space groups and anion−cation arrangements of the ionic crystals of the Keggin-type polyoxometalates are different from each other, and the effects of the anion charges on the crystal structures and sorption properties are unclear.

The molecular size and symmetry of α-Dawson-type polyoxometalates[10] (parts b−d of Figure 1) are different from those of α-Keggin-type polyoxometalates (Figure 1a) with T_d symmetry. α-Dawson-type polyoxometalates have D_{3h} symmetry, and two kinds of $[WO_6]$ units are located in the cap and belt positions, and those with higher anion charges can be synthesized by the substitution of $[WO_6]$ units with $[VO_6]$ units (parts c and d of Figure 1).

In this work, we report the crystal structures and sorption properties of the ionic crystals of the α-Dawson-type polyoxometalates with the $[Cr_3O(OOCH)_6(H_2O)_3]^+$ macrocation. The $[\alpha\text{-}P_2W_{18}O_{62}]^{6-}$, $[\alpha_2\text{-}P_2W_{17}V_1O_{62}]^{7-}$, and $[\alpha\text{-}P_2W_{15}V_3O_{62}]^{9-}$ polyoxometalates with different anion charges are used, and the effects of the anion charges on the crystal structures and sorption properties of the ionic crystals are investigated.

Experimental Section

Syntheses of the Ionic Crystals. All the starting materials were reagent grade and used as purchased. Ammonium salts of the Dawson-type polyoxometalates $(NH_4)_6[\alpha\text{-}P_2W_{18}O_{62}]\cdot 14H_2O$,[10c] $(NH_4)_7[\alpha_2\text{-}P_2W_{17}V_1O_{62}]\cdot 16H_2O$,[10d] and $(NH_4)_9[\alpha\text{-}P_2W_{15}V_3O_{62}]\cdot 16H_2O$,[10e] were synthesized and characterized by Fourier transform (FT)-IR and ^{31}P NMR spectroscopy according to the literatures. IR spectrum of $(NH_4)_6[\alpha\text{-}P_2W_{18}O_{62}]$ (KBr): 1400, 1090, 1019, 959, 912, and 776 cm^{-1}. ^{31}P NMR of $(NH_4)_6[\alpha\text{-}P_2W_{18}O_{62}]$ (D_2O): −12.4 ppm. IR spectrum of $(NH_4)_7[\alpha_2\text{-}P_2W_{17}V_1O_{62}]$ (KBr): 1400, 1086, 954, 917, and 786 cm^{-1}. ^{31}P NMR of $(NH_4)_7[\alpha_2\text{-}P_2W_{17}V_1O_{62}]$ (D_2O): −11.2 and −3.3 ppm. IR spectrum of $(NH_4)_9[\alpha\text{-}P_2W_{15}V_3O_{62}]$ (KBr): 1400, 1082, 1052, 1018, 941, 917, 894, and 782 cm^{-1}. ^{31}P NMR of $(NH_4)_9[\alpha\text{-}P_2W_{15}V_3O_{62}]$ (D_2O): −6.4 and −13.4 ppm. The formate salt of the macrocation $[Cr_3O(OOCH)_6(H_2O)_3](OOCH)\cdot nH_2O$[12] was synthesized and characterized by FT-IR spectroscopy according to the literature. IR spectrum of $[Cr_3O(OOCH)_6(H_2O)_3]$-(OOCH) (KBr): 1635, 1575, 1377, 1317, and 660 cm^{-1}.

$(NH_4)_4[Cr_3O(OOCH)_6(H_2O)_3]_2[\alpha\text{-}P_2W_{18}O_{62}]\cdot 15H_2O$ (**1a**) was synthesized as follows: $[Cr_3O(OOCH)_6(H_2O)_3](OOCH)\cdot nH_2O$ (0.20 g, ca. 0.35 mmol) and $(NH_4)_6[\alpha\text{-}P_2W_{18}O_{62}]\cdot 14H_2O$ (1.0 g, 0.21 mmol) were dissolved into 20 mL of 0.01 M HNO_3 (pH 2) and NH_4Cl (0.25 g, 4.8 mmol) was added. Then the solution was kept at 288 K for 24 h. Green crystals of **1a** were isolated in 42% yield. IR spectrum (KBr): 1397 (sh, δ(NH)), 1375 (vs, ν_{sym}(OCO)), 1092 (s, ν_{asym}(P−O)), 962 (vs, ν_{asym}(W═O)), 905 (vs, ν_{asym}(W−Oc−W)), and 789 cm^{-1} (vs, ν_{asym}(W−Oe−W)). Elemental analysis calcd. for $C_{12}H_{70}N_4O_{109}P_2W_{18}Cr_6$: C, 2.53; H, 1.24; N, 0.98; P, 1.09; W, 58.08; Cr, 5.48. Found: C, 2.36; H, 1.26; N, 1.07; P, 1.08; W, 58.17; Cr, 5.38.

$(NH_4)_5[Cr_3O(OOCH)_6(H_2O)_3]_2[\alpha_2\text{-}P_2W_{17}V_1O_{62}]\cdot 15H_2O$ (**2a**) was synthesized as follows: $[Cr_3O(OOCH)_6(H_2O)_3](OOCH)\cdot nH_2O$ (0.20 g, ca. 0.35 mmol) and $(NH_4)_7[\alpha_2\text{-}P_2W_{17}V_1O_{62}]\cdot 16H_2O$ (1.0 g, 0.22 mmol) were dissolved into 20 mL of 0.01 M HNO_3 (pH 2) and NH_4Cl (0.10 g, 1.9 mmol) was added. Then the solution was kept at 293 K for 24 h. Green crystals of **2a** were isolated in 70% yield. IR spectrum (KBr): 1400 (s, δ(NH)), 1375 (vs, ν_{sym}(OCO)), 1087 (s, ν_{asym}(P−O)), 955 (vs, ν_{asym}(W═O)), 910 (vs, ν_{asym}(W−Oc−W)), 786 cm^{-1} (vs, ν_{asym}(W−Oe−W)). Elemental analysis calcd. for $C_{12}H_{74}N_5O_{109}P_2W_{17}V_1Cr_6$: C, 2.58; H, 1.33; N, 1.25; P, 1.11; W, 55.99; V, 0.91; Cr, 5.59. Found: C, 2.70; H, 1.30; N, 1.25; P, 1.15; W, 55.48; V, 0.89; Cr, 5.63.

$(NH_4)_7[Cr_3O(OOCH)_6(H_2O)_3]_2[\alpha\text{-}P_2W_{15}V_3O_{62}]\cdot 15H_2O$ (**3a**) was synthesized as follows: $[Cr_3O(OOCH)_6(H_2O)_3](OOCH)\cdot nH_2O$ (0.20 g, ca. 0.35 mmol) and $(NH_4)_9[\alpha\text{-}P_2W_{15}V_3O_{62}]\cdot 16H_2O$ (1.00 g, 0.23 mmol) were dissolved in 20 mL of 0.03 M HNO_3 (pH 1.5), and NH_4Cl (0.30 g, 5.7 mmol) was added. Then the solution was kept at 293 K for 24 h. Dark-brown crystals of **2a** were isolated in 80% yield. IR spectrum (KBr): 1399 (s, δ(NH)), 1377 (vs, ν_{sym}(OCO)), 1082 (s, ν_{asym}(P−O)), 1051 (m), 1035 (m), 1011 (m), 938 (s), 910

(6) (a) Pope, M. T.; Müller, A. *Angew. Chem. Int. Ed.* **1991**, *30*, 34. (b) Hölscher, M.; Englert, U.; Zibrowius, B.; Hölderich, W. F. *Angew. Chem. Int. Ed.* **1994**, *33*, 2491. (c) Khan, M. I.; Yohannes, E.; Powell, D. *Inorg. Chem.* **1999**, *38*, 212. (d) Hagrman D.; Hagrman, P. J.; Zubieta, J. *Angew. Chem. Int. Ed.* **1999**, *38*, 3165. (e) Son, J. H.; Choi, H.; Kwon, Y. U. *J. Am. Chem. Soc.* **2000**, *122*, 7432. (f) du Peloux, C.; Dolbecq, A.; Mialane, P.; Marrot, J.; Rivière, E.; Sécheresse, F. *Angew. Chem. Int. Ed.* **2001**, *40*, 2455. (g) Forment-Aliaga, A.; Coronado, E.; Feliz, M.; Gaita-Arino, A.; Llusar, R.; Romero, F. M. *Inorg. Chem.* **2003**, *42*, 8019. (h) Fukaya, K.; Yamase, T. *Angew. Chem. Int. Ed.* **2003**, *42*, 654. (i) Müller, A.; Das, S. K.; Talismanov, S.; Roy, S.; Beckmann, E.; Bögge, H.; Schmidtmann, M.; Merca, A.; Berkle, A.; Allouche, L.; Zhou, Y.; Zhang, L. *Angew. Chem. Int. Ed.* **2003**, *42*, 5039. (j) Ishii, Y.; Takenaka, Y.; Konishi, K. *Angew. Chem. Int. Ed.* **2004**, *43*, 2702.
(7) (a) Okuhara, T.; Mizuno, N.; Misono, M. *Adv. Catal.* **1996**, *41*, 113. (b) Hill, C. L. *Chem. Rev.* **1998**, *98*, 1. (c) Neumann, R. *Prog. Inorg. Chem.* **1998**, *47*, 317. (d) Kozhevnikov, I. V. *Catalysis by Polyoxometalates*; Wiley: Chichester, England, 2002.
(8) (a) Uchida, S.; Hashimoto, M.; Mizuno, N. *Angew. Chem. Int. Ed.* **2002**, *41*, 2814. (b) Uchida, S.; Mizuno, N. *Chem.−Eur. J.* **2003**, *9*, 5850.
(9) Uchida, S.; Mizuno, N. *J. Am. Chem. Soc.* **2004**, *126*, 1602.
(10) (a) Dawson, B. *Acta Crystallogr.* **1953**, *6*, 113. (b) Contant, R.; Thouvenot, R. *Inorg. Chim. Acta* **1993**, *212*, 41. (c) Contant, R. *Inorg. Synth.* **1990**, *27*, 105. (d) Abbesi, M.; Contant, R.; Thouvenot, R.; Hervé, G. *Inorg. Chem.* **1991**, *30*, 1695. (e) Harmalker, S. P.; Leparulo, M. A.; Pope, M. T. *J. Am. Chem. Soc.* **1983**, *105*, 4286.
(11) Johnson, M. K.; Powell, D. B.; Cannon, R. D. *Specrochim. Acta* **1981**, *37A*, 995.
(12) Onishi, H. *Photomeric Determination of Traces of Metals*; John-Wiley: New York, 1986.

(m), 887 (m), 785 (br) cm^{-1}. Elemental analysis calcd. for $C_6H_{82}N_7O_{109}P_2W_{15}V_3Cr_6$: C, 2.67; H, 1.64; N, 1.81; P, 1.15; W, 51.00; V, 2.83; Cr, 5.77. Found: C, 2.37; H, 1.58; N, 1.81; P, 1.16; W, 51.51; V, 2.86; Cr, 5.83.

The compounds **1a**−**3a** were dissolved into water, and the amounts of polyoxometalates in **1a**−**3a** were determined by the intensities of 250-nm (oxygen to tungsten charge transfer) bands.[9e] Cr(III) in the macrocation was converted to $[CrO_4]^{2-}$ by the addition of H_2O_2 and aqueous sodium hydroxide solution into the aqueous solution of **1a**−**3a**, and the amounts of chromium in **1a**−**3a** were determined by the intensities of 366-nm (oxygen to chromium charge transfer) bands.[12] The UV−vis data showed that the macrocation/polyoxometalate ratios in **1a**, **2a**, and **3a** were calculated as 2.0:1.0, 2.1:1.0, and 1.9:1.0, respectively, and the values fairly agreed with those of the elemental analyses.

Preparation of Guest-Free Phases of 1a−3a. The water of crystallization in **1a**−**3a** was desorbed by the evacuation or heat treatment in an N_2 flow at 373 K to form the corresponding guest-free phases of **1b**−**3b**, respectively. The weight losses for **1a**−**3a** after the treatments were 4.9, 4.9, and 5.0%, respectively. The values fairly agreed with the amounts of the water of crystallization in **1a**−**3a** (**1a**, 4.7%; **2a**, 4.8%; **3a**, 5.0%), showing that the water of crystallization is almost removed by the treatment. The peak positions of the powder X-ray diffraction (XRD) patterns of **1b**−**3b** were restored to those of **1a**−**3a** by the exposure to the saturated water vapor. Therefore, the structure transformation between **1a**−**3a** and **1b**−**3b** proceeds reversibly. The IR spectra of **1b**−**3b** showed characteristic bands of the ammonium ions, macrocations, and polyoxometalates, showing that the molecular structures of the constituent ions are maintained upon the loss of the water of crystallization.

Single-Crystal X-ray Analyses. The diffraction measurement of **1a** was performed on a Rigaku AFC7R automated four-circle diffractometer. A Mo X-ray source equipped with a graphite-monochromated Mo Kα radiation ($\lambda = 0.71069$ Å) was used. The unit cell was determined and refined by a least-squares method using 25 independent reflections ($20 < 2\theta < 25°$). Data were collected with a ω-2θ scan technique at room temperature. Three standard reflections were monitored at every 150 measurements. In the reduction of the data, Lorentz polarization corrections and an empirical absorption correction (ψ scan) were made. The structure analysis was performed by using the CrystalStructure crystallographic program package.[13] The structure of **1a** was solved by the direct methods (SIR-92)[14] and expanded using Fourier synthesis (DIRDIF99).[15] In the final cycle of the full-matrix least-squares refinement, tungsten and oxygen atoms of the polyoxometalate were refined anisotropically. The chromium atoms of the macrocations in the column I (see the results and discussion section) were also refined anisotropically. The chromium atoms of the macrocations in the column II (see the results and discussion section) had the occupancy of 0.5, were disordered over the two positions within the *ab* plane, and were refined isotropically. The nitrogen atom of the ammonium ions had the occupancy of $^2/_3$ and was refined isotropically. The other non-hydrogen atoms were refined isotropically. Neutral scattering factors were obtained from the standard source.[16]

The diffraction measurements of **2a** and **3a** were performed on a Rigaku Mercury diffractometer equipped with a charge-coupled device area detector. Crystallographic data of compound **2a** were as follows: trigonal *P*-3, $a = 15.984$ Å, $c = 21.611$ Å, $V = 4781.7$ Å^3, $Z = 2$, $R_1 = 0.171$, $wR_2 = 0.191$. Crystallographic data of compound **3a** were as follows: trigonal *P*-3, $a = 15.957$ Å, $c = 20.922$ Å, $V = 4613.7$ Å^3, $Z = 2$, $R_1 = 0.133$, $wR_2 = 0.145$. The positions of the $[VO_6]$ units in **2a** and **3a** could not be determined by the disordering with the $[WO_6]$ units. The macrocations were disordered between the two positions along the *c* axis while the average position was the same as that in **1a** (at the center of the surrounded polyoxometalates). The crystal structures of **2a** and **3a** could also be solved with hexagonal $P6_3/m$, which was observed for **1a**, while trigonal *P*-3 gave lower *R* values. The positions of the atoms determined by the analyses with the two different space groups agreed approximately with each other (within ±0.3 Å).

Powder X-ray Diffraction Analyses. Powder XRD patterns were measured with XRD-DSCII (Rigaku Corporation) and Cu Kα radiation ($\lambda = 1.54056$ Å, 50 kV, 200 mA). The data were collected in the range of $2\theta = 3-38°$ (at 0.01° point and 0.25° min^{-1} for **1a**−**3a**, and 0.10° min^{-1} for **1b**−**3b**). The measurements for **1a**−**3a** were performed in air at 303 K, and those for **1b**−**3b** were performed in a dry N_2 flow (300 mL min^{-1}) at 373 K. The crystal structures were elucidated using Material Studio (Accelrys Inc.). The X-ray scattering of ammonium ions and water molecules was much lower compared to that of polyoxometalates and macrocations containing heavy atoms (tungsten and chromium) and was negligible.[17] Therefore, ammonium ions and water of crystallization were omitted from the calculation. The calculation was performed as follows: (1) unit cell indexing and space-group determination using X-cell;[18] (2) peak profile fitting using Pawley refinement;[19] (3) a starting model was created by arranging the polyoxometalates and macrocations in the unit cell, the calculated powder XRD pattern was compared to the experimental data, and the model was optimized by the simulated annealing method;[20] and (4) final structure refinement using the Rietveld method.[21] The validity of the calculation was checked in the case of **1a** whose crystal structure was independently determined by the single-crystal X-ray analysis. The *R*wp values $[\Sigma w(y_i - f_i)^2/\Sigma w(f_i^2)^2]^{1/2}$, where y_i and f_i are the experimental and calculated diffraction intensity, respectively, were shown in parentheses: **1a** (15.60%), **1b** (11.51%), **2a** (13.09%), **2b** (14.17%), **3a** (19.61%), and **3b** (11.41%). The space groups were $P6_3/m$, and the arrangements of the polyoxometalates and macrocations in **2a**, **2b**, and **1b**−**3b** were the same as that in **1a**. The lattice constants of **1a**−**3a** agreed with those (within ±0.08 Å) obtained with the single-crystal X-ray analyses.

Characterization. FT-IR spectra were recorded on KBr pellets with a Paragon 1000 PC spectrometer (Perkin-Elmer). The measurements of TG-DTA and water sorption kinetics (at constant water vapor pressures) were carried out with Thermo Plus 2 (Rigaku Corporation) using α-Al_2O_3 as a reference. In the TG-DTA measurements, the evolved gas was analyzed by the mass spectrometer system (GCMS-QP5050A, Shimadzu). The vapor sorption isotherms of **1b**−**3b** were measured with an automatic sorption apparatus (Hydrosorb (water) and Autosorb (alcohols), Quantachrome Corporation). The P_0 values were the saturation pressures of the sorbents at 298 K and were shown in parentheses; water (3.06

(13) *CrystalStructure 3.60, Structure solution, refinement, and reporting software*; Rigaku/MSC, 2004.
(14) Altomare, A.; Cascarano, G.; Giacovazzo, C.; Guagliardi, A.; Burla, M. C.; Polidori, G.; Camalli, M. *J. Appl. Crystallogr.* **1994**, *27*, 435.
(15) Beuskens, P. T.; Admiraal, G.; Beurskens, G.; Bosman, W. P.; de Gelder, R.; Israel, R.; Smits, J. M. M. *DIRDIF99*; University of Nijmegen: Nijmegen, The Netherlands, 1999.
(16) *International Tables for X-ray Crystallography*; Kynoch Press: Birmingham, 1974; Vol. 4.
(17) Chantler, C. T. *J. Phys. Chem. Ref. Data* **2000**, *29*, 597.
(18) Neumann, M. A. *J. Appl. Crystallogr.* **2003**, *36*, 356.
(19) Pawley, G. S. *J. Appl. Crystallogr.* **1981**, *14*, 357.
(20) Engel, G. E.; Wilke, S.; König, O.; Harris, K. D. M.; Leusen, F. J. J. *J. Appl. Crystallogr.* **1999**, *32*, 1169.
(21) Rietveld, H. M. *J. Appl. Crystallogr.* **1969**, *2*, 65.

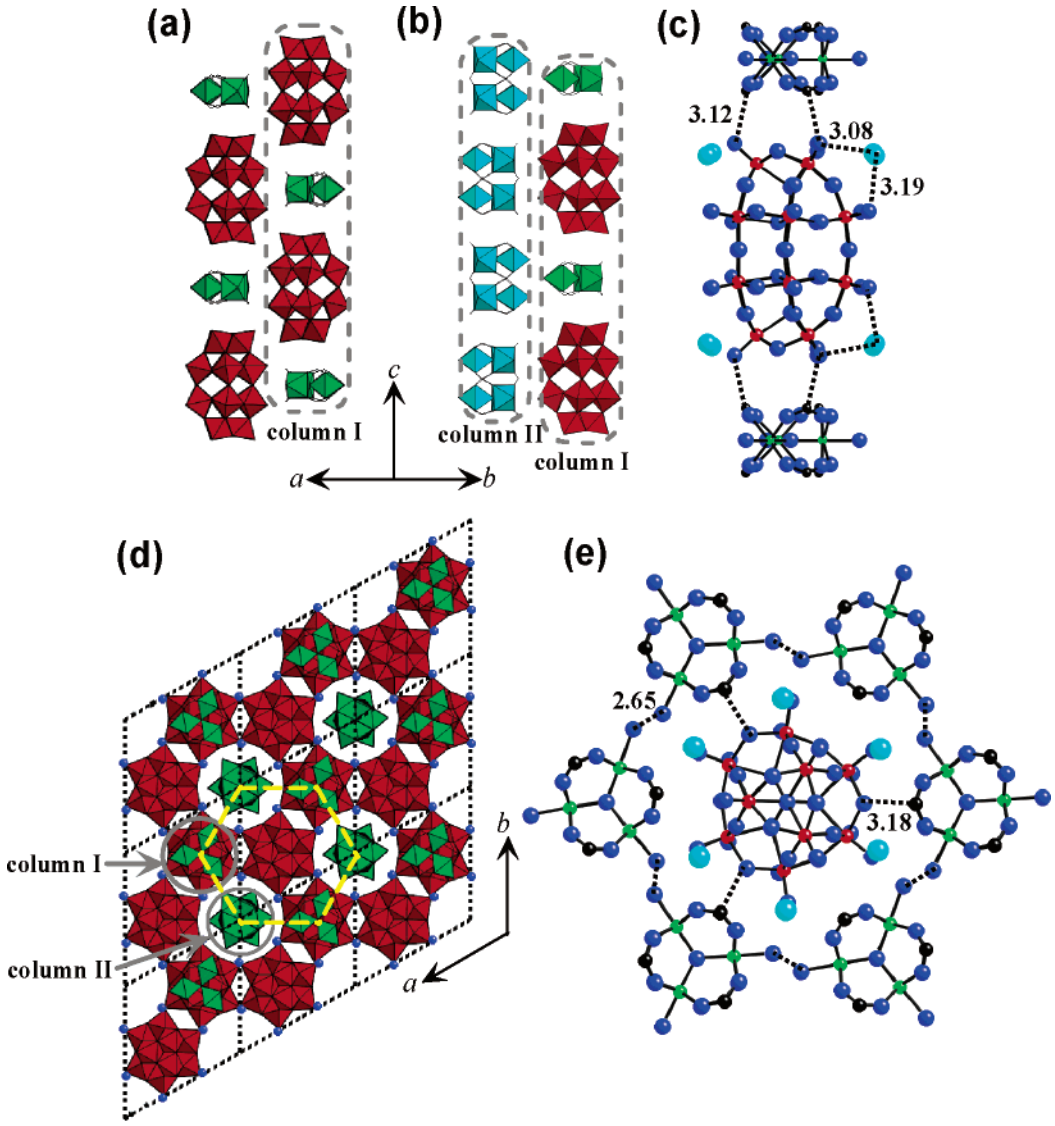

Figure 2. Crystal structure of **1a**. (a) Arrangements of the constituent ions in column I and (b) those in column II with respect to column I. Red and green polyhedra showed the $[WO_6]$ units of the polyoxometalate and the $[CrO_6]$ units of the macrocation, respectively. Blue spheres showed the NH_4^+. $[CrO_6]$ units of the macrocation in column II were shown by the light-blue polyhedra and the occupancy of each macrocation was 0.5. (c) Ball and stick model of the constituent ions showing the anion−cation arrangements in column I. Light blue spheres, NH_4^+; red spheres, W; blue spheres, oxygen; black spheres, carbon; green spheres, chromium. (d) Arrangements of the constituent ions in the *ab* plane and (e) ball and stick model of the local structure of the yellow hexagon in part d in the *ab* plane. Broken lines in parts c and e showed the hydrogen bonds.

kPa), methanol (15.6 kPa), ethanol (6.67 kPa), and 1-propanol (2.67 kPa).

Results and Discussion

Syntheses. Selection of the countercation was an important factor for the complexation of the Dawson-type polyoxometalates with the macrocation. The addition of KCl and RbCl gave the compounds with poor crystallinity, while the addition of CsCl gave the cesium salts of the corresponding polyoxometalates. Only the addition of NH_4Cl gave compounds with the good crystallinity. The FT-IR spectra of **1a**−**3a** showed bands characteristic of the polyoxometalates and macrocation, showing that the molecular structures of the constituent ions for **1a**−**3a** are maintained. Elemental analyses of **1a**−**3a** showed that the macrocation/polyoxometalate ratios were 2:1 for **1a**−**3a**. While the macrocation/polyoxometalate ratio in the synthetic solution was changed from 4:1 to 1:4, the stoichiometry in the complexes formed was the same as that of **1a**.

Table 1. Crystallographic Data for 1a

formula	$C_{12}O_{100}Cr_6W_{18}P_2N_4$
formula weight	5483.32
cryst syst	hexagonal
space group	$P6_3/m$
a, Å	16.009(4)
c, Å	21.785(9)
V, Å^3	4835(2)
Z	2
D_c, g cm^{-3}	3.766
crystal size, mm	0.2 × 0.2 × 0.01
temp, K	296.1
μ(Mo Kα), cm^{-1}	221.36
no. measd reflections	4220
no. obsd reflections	2320 ($I > 3\sigma(I)$)
no. parameters refined	190
R_1, wR_{2a}	0.042, 0.045

[a] $R_1 = \Sigma||F_o| - |F_c||/\Sigma|F_o|$; $wR_2 = [\Sigma w(F_o - F_c)^2/\Sigma wF_o^2]^{1/2}$.

Crystal Structures of 1a−3a. The crystal structure and the crystallographic data of **1a** are shown in Figure 2 and Table 1, respectively. The structure of **1a** was well described

Table 2. Lattice Constants and Volumes of 1a−3a and 1b−3b[a]

	1a	1b	2a	2b	3a	3b
a, Å	16.009	15.524	15.984	15.588	15.957	15.791
c, Å	21.785	20.744	21.611	20.487	20.922	18.836
V, Å^3	4835	4329	4781	4311	4613	4067

[a] Lattice constants (*a*, *c*, *V*) of **1a**, **2a**, and **3a** were obtained from the single-crystal X-ray analyses, and those of **1b**, **2b**, and **3b** were calculated from the powder XRD patterns.

by the two types of columns (I and II) running along the *c* axis. Column I (Figure 2a) was composed of polyoxometalates and macrocations that were placed alternatively along the *c* axis. Column II (Figure 2b) contained only macrocations that were disordered between the two positions along the *c* axis with an occupancy of 0.5. As shown in Figure 2c, the distance between the carbon atoms of the bridging formates in the macrocations and the terminal oxygen atoms of the polyoxometalates along the *c* axis was 3.12 Å, and within hydrogen-bonding distance. The polyoxometalate existed just at the center of the neighboring macrocations in column I. The ammonium ions existed in the vicinity of the terminal oxygen atoms of the polyoxometalates with distances of 3.08 Å and 3.19 Å. As shown in Figure 2d, column I assembled to form a honeycomb in the *ab* plane and the column II existed inside the honeycomb. Thus, the symmetry of the polyoxometalates (D_{3h}) and macrocations (D_{3h}) reflected on the crystal structure of **1a** (hexagonal, $P6_3/m$). As shown in Figure 2e, the distance between the oxygen atoms of the aquo-ligands of the macrocations of columns I and II was 2.65 Å. The distance between the carbon atoms of the bridging formates of the macrocations in column II and the bridging oxygen atoms of the polyoxometalates in the column I was 3.18 Å. Thus, multiple hydrogen bonds existed between the columns. The multiple hydrogen bonds among the constituent ions probably contribute to the stabilization of the crystal structure of **1a**. The data of TG-DTA and elemental analyses showed the existence of fifteen water molecules of the crystallization per formula unit, and the positions of six water molecules were confirmed by the single-crystal X-ray analysis. The remaining water molecules are probably highly disordered.

The experimental powder XRD patterns of **1a**−**3a** are shown in parts a−c of Figure 3, respectively. The lattice constants obtained by the calculation are summarized in Table 2. While the lengths of the *a* axes were almost the same among **1a**−**3a** (15.984−16.009 Å), those of the *c* axes decreased in the order of **1a** (21.785 Å) ≥ **2a** (21.611 Å) > **3a** (20.922 Å). The decrease in the *c* axes is probably due to the increase in the anion−cation interaction with increase in the anion charge.

Crystal Structures of 1b−3b. Parts a−c of Figure 4 show the experimental powder XRD patterns of **1b**−**3b**, respectively. The peak positions shifted to the higher angles upon the loss of the water of crystallization. The experimental patterns of **1b**−**3b** were well reproduced by the calculations with structural models of the honeycomb packing of the polyoxometalates and macrocations as shown by the dotted lines. The lattice constants obtained by the calculation are summarized in Table 2. While the lengths of the *a* axes were almost the same among **1b**−**3b** (15.524−15.791 Å), those

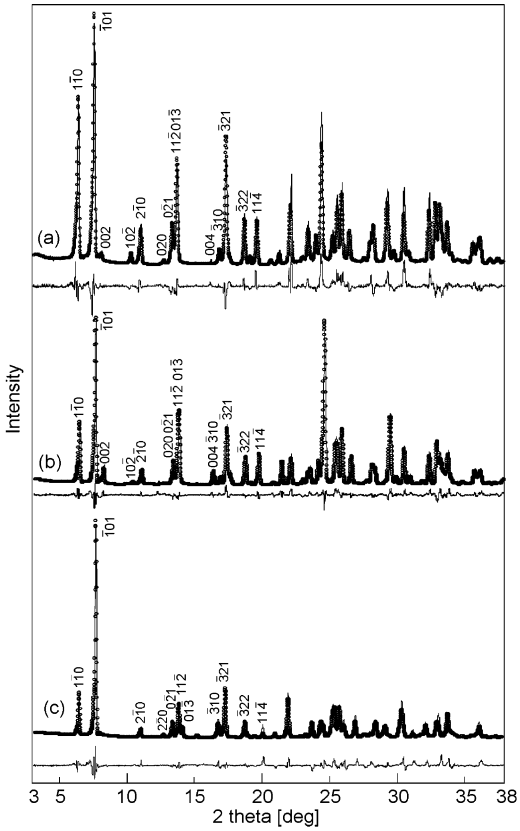

Figure 3. Powder XRD patterns of (a) **1a**, (b) **2a**, and (c) **3a**. The figure showed the Miller index of each reflection (2θ < 20°). The calculated patterns (dotted lines) were overlaid with the experimental patterns (solid lines). The difference between the experimental and calculated data was shown under the patterns.

of the *c* axes decreased in the order of **1b** (20.744 Å) ≥ **2b** (20.487 Å) > **3b** (18.836 Å). The decrease in the *c* axes is possibly explained by the increase in the anion−cation interaction with increase in the anion charge as that for **1a**−**3a**.

The changes in the lengths of the *c* axes from **1a**−**3a** to **1b**−**3b** were −1.041 Å, −1.124 Å, and −2.086 Å, respectively, and the reduction from **3a** to **3b** was much larger than those from **1a**−**2a** to **1b**−**2b**. The changes in the lengths of the *c* axes were much larger than those of the *a* axes (−0.166 to −0.485 Å). Similar changes were observed when **1b** and **3b** were exposed to the water vapor at $P/P_0 = 0.7$: The length of the *a* and *c* axes of **1b** were lengthened by 0.3−0.5 Å, while the *a* and *c* axes of **3b** were lengthened by 0.5 and 2.0 Å, respectively, and the *c* axis was more lengthened.

Parts a−c of Figure 5 show the space-filling models of the arrangements of the column I along the *c* axis in **1b**−**3b**, respectively. The compounds **1b**−**3b** possessed voids running perpendicular to the *c* axis and had no voids in the *ab* plane (Figure S1). In Figure 5, voids with the widest openings were indicated by the broken circles. The widest voids were created between the oxygen atoms of the polyoxometalates of the neighboring columns. The cross section diameters decreased in the order of **1b** (3.85 Å) > **2b** (3.56 Å) > **3b** (3.29 Å).[22] The decrease in the sizes of the voids is probably due to the increase in the anion−cation interaction. The sizes of the voids are comparable to or larger than the diameter of the water molecule (3.10 Å).[23]

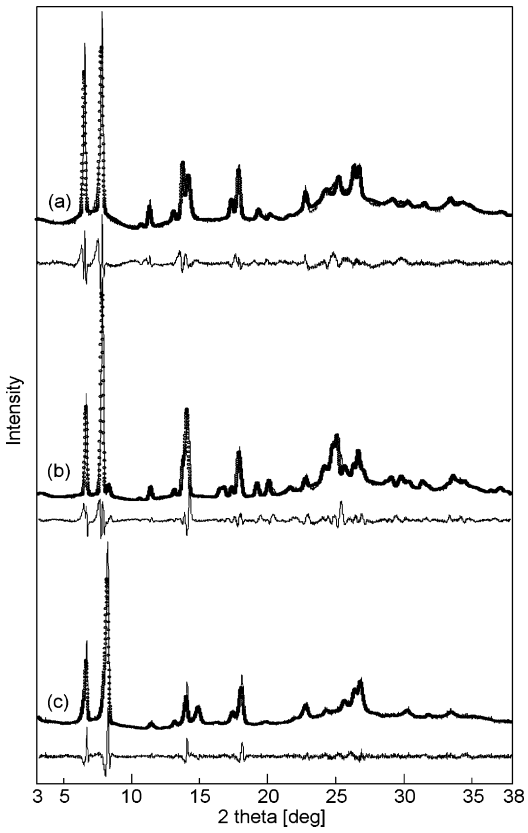

Figure 4. Powder XRD patterns of (a) **1b**, (b) **2b**, and (c) **3b**. The calculated patterns (dotted lines) were overlaid with the experimental patterns (solid lines). The difference between the experimental and calculated data was shown under the patterns.

Water and Alcohol Sorption Properties of 1b−3b. Figure 6 shows the water sorption isotherms of **1b**−**3b** at 298 K. Steep uptakes were observed for the isotherms of **1b**−**3b** at the low pressures. The isotherms of **1b** and **2b** showed plateaus, while the amount of sorption for **3b** gradually increased with the increase in the vapor pressure. The amounts of sorption for **1b**−**3b** around the saturation pressure (298 K) were 15 mol/mol (65 $cm^3\ g^{-1}$), 16 mol/mol (69 $cm^3\ g^{-1}$), and 20 mol/mol (87 $cm^3\ g^{-1}$), respectively, and were close to that (15 mol/mol) of the water of crystallization in **1a**−**3a**.

The water sorption energies of **1b**−**3b** were calculated from the water sorption isotherms by using the Clausius−Clapeyron equation[25] (Figures S2−S4 in Supporting Information). The water sorption energies of **1b** and **2b** were ca. −30 and −32 kJ mol^{-1}, respectively, and did not much change with the amounts of sorption. The values were smaller than the heat of condensation at 298 K (−44 kJ mol^{-1}) and in the range of the physical adsorption.[26] The water sorption energy of **3b** was smaller than the heat of condensation at the small amounts of sorption, gradually increased, and became larger than −60 kJ mol^{-1} beyond 9 mol/mol (40 $cm^3\ g^{-1}$). Therefore, the water sorption thermodynamics of **3b** was probably different from those of **1b** and **2b**.

To gain information on the water sorption kinetics, changes in the amounts of water sorption for the compounds as a function of time were measured. The water sorption profiles of only **1b** and **3b** were investigated since the water sorption isotherms and energies of **1b** and **2b** were close to each other. In many cases, guest sorption on microporous materials can be reproduced by the linear driving force mass transfer model[27]

$$M_t = M_e\{1 - \exp(-k_1 t)\} \quad (1)$$

where M_t and M_e are the amounts of sorption at time t and equilibrium, respectively, and k_1 is the rate constant. Figure 7a shows the experimental and calculated data for **1b**. The experimental data were well reproduced with $M_e = 12.2$ mol/mol (50.3 $cm^3\ g^{-1}$) and $k_1 = 2.9 \times 10^{-4}\ s^{-1}$.

The experimental data of **3b** shown in Figure 7b could not be reproduced by eq 1. Therefore, two kinds of barriers (eq 2) were considered for the water sorption kinetics of **3b**, as in the case of the alcohol sorption for the Ni−bipyridine compound reported by Fletcher et al.[28]

$$M_t = M_{e_1}\{1 - \exp(-k_1 t)\} + M_{e_2}\{1 - \exp(-k_2 t)\} \quad (2)$$

where M_{e_1} and M_{e_2} are the contributions of each of the two processes controlling the overall sorption (i.e., $M_{e_1} + M_{e_2} = M_e$: amounts of sorption at equilibrium), and k_1 and k_2 are the rate constants. The experimental data were well reproduced with $M_{e_1} = 9.0$ mol/mol (39.6 $cm^3\ g^{-1}$), $k_1 = 1.3 \times 10^{-3}\ s^{-1}$, $M_{e_2} = 1.3$ mol/mol (5.7 $cm^3\ g^{-1}$), and $k_2 = 1.4 \times 10^{-4}\ s^{-1}$.

As shown in Figure 7b, the contribution of k_1 to the water sorption for **3b** was larger, and then that of k_2 probably reflects the main process in the water sorption. As shown in Figure 5, both **1b** and **3b** possessed voids whose sizes were comparable to or larger than that of water molecules. Therefore, k_1 probably describes the diffusion of water molecules into the voids of **1b** and **3b**. The k_1 value for **3b** was larger than that for **1b**, while the void of **3b** was smaller than that of **1b**. This may be related to the larger anion charge and amounts of ammonium ions per unit volume for **3b** than those for **1b** because the diffusion constants of small alcohol molecules into $(NH_4)_4SiW_{12}O_{40}$ were larger than those into $(NH_4)_3PW_{12}O_{40}$, although the sizes of the micropores were the same.[29] On the other hand, k_2 was needed only for **3b**, and the value was smaller than k_1. The rate constant k_2 probably describes the large expansion in the c axis of **3b**.

(22) The cross-section diameters of the voids were estimated by drawing the space-filling model of the crystal structures with the van der Waals radii (oxygen, 1.50 Å; carbon, 1.70 Å; tungsten, 1.41 Å; phosphorous, 1.85 Å) or ionic radii (NH_4^+, 1.51 Å; Cr(III), 0.76 Å).
(23) The cross-section diameter of the molecule was defined as the diameter of the circumscribed circle of the smallest cross section of the molecular model. The molecular models of water and alcohol molecules were drawn with the van der Waals radii of the elements. The cross-section diameters for water, methanol, and ethanol were 3.10, 3.85, and 4.45 Å, respectively. These values agreed with those reported in ref 24.
(24) McClellan, A. L.; Harnsberger, H. F. *J. Colloid Interface Sci.* **1967**, *23*, 577.
(25) Atkins, P. W. *Physical Chemistry*; Oxford University Press: Oxford, 1990; Chapter 29.
(26) Stull, D. R.; Westrum, E. F.; Sinke, G. C. *The Chemical Thermodynamics of Organic Compounds*; John Wiley and Sons: New York, 1969.
(27) (a) Foley, N. J.; Thomas, K. M.; Forshaw, P. L.; Stanton, D.; Norman, P. R. *Langmuir* **1997**, *13*, 2083. (b) Eddaudi, M.; Li, H.; Yaghi, O. M. *J. Am. Chem. Soc.* **2000**, *122*, 1391.
(28) Fletcher, A. J.; Cussen, E. J.; Bradshaw, D.; Rosseinsky, M. J.; Thomas, K. M. *J. Am. Chem. Soc.* **2004**, *126*, 9750.
(29) Nayak, V. S.; Moffat, J. B. *J. Phys. Chem.* **1988**, *92*, 7097.

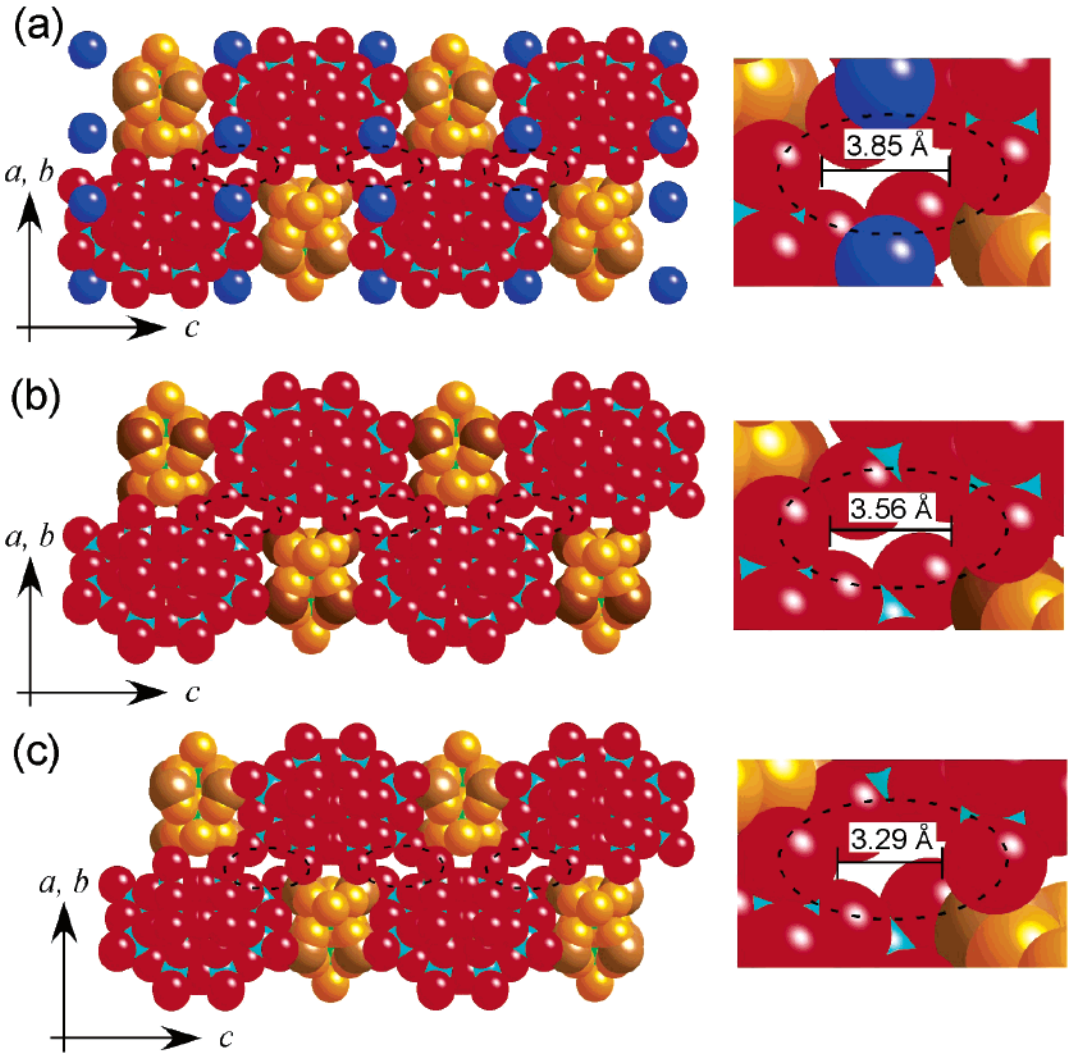

Figure 5. Space-filling models showing the arrangements of the constituent ions in column I for (a) **1b**, (b) **2b**, and (b) **3b**. Red, light-blue, orange, brown, and blue spheres showed the oxygen atom of the polyoxometalate, tungsten (vanadium), oxygen atom of the macrocation, carbon, and nitrogen, respectively. As for compounds **2b** and **3b**, the positions of the nitrogen atoms (of the ammonium ions) were not determined and not shown (see the Experimental Section). Broken lines indicated the voids. The models at the right showed the magnified views.

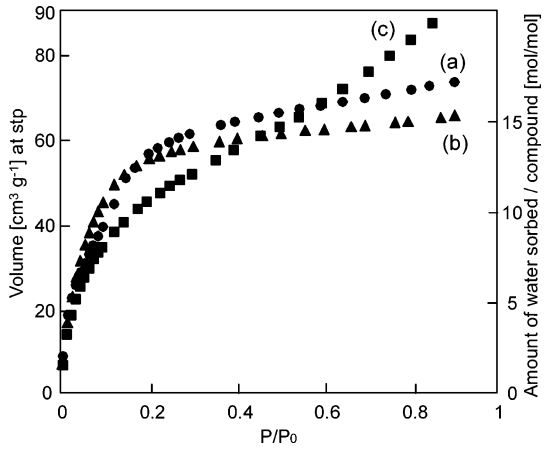

Figure 6. Water sorption isotherms of (a) **1b** (●), (b) **2b** (▲), and (c) **3b** (■) at 298 K.

To expand the *c* axis of **3b**, the distance between the polyoxometalates and macrocations needs to increase, and the expansion would show a higher barrier compared to the diffusion of water molecules into the voids. The expansion of the lattice is promoted by the ion−dipole interaction between the host−guest as previously reported,[8] and the water of crystallization in **1a** interacted with the ammonium ions. Since the anion charge and amounts of ammonium ions of **3b** are larger than those of **1b**, the ion−dipole interaction between the host−guest of **3b** would be larger than that of **1b**. The larger ion−dipole interaction of **3b** would promote the expansion in the *c* axis with the water sorption.

Next, the alcohol sorption properties of **1b**−**3b** were considered. Parts a−c of Figure 8 show the methanol sorption isotherms of **1b**−**3b**, respectively. The sorption isotherm of **1b** started at the very low pressures, while gate pressures were observed for **2b** and **3b**. Parts a−c of Figure 9 show the ethanol sorption isotherms of **1b**−**3b**, respectively. The compound **3b** excluded ethanol, and **2b** sorbed only a small amount (up to ca. 2.5 mol/mol (10 cm^3 g^{-1})) of ethanol at the high pressures. The compound **1b** showed a gate pressure in the ethanol sorption. In general, the gate pressure exists when the sizes of the guest molecules are larger than the openings of the voids, and the guest sorption is accompanied by the structural change of the host solid to accommodate the guests.[30] The diameters of water, methanol, and ethanol molecules are 3.10, 3.89, and 4.45 Å, respectively.[23] Since the size of the void of **1b** is comparable to that of the

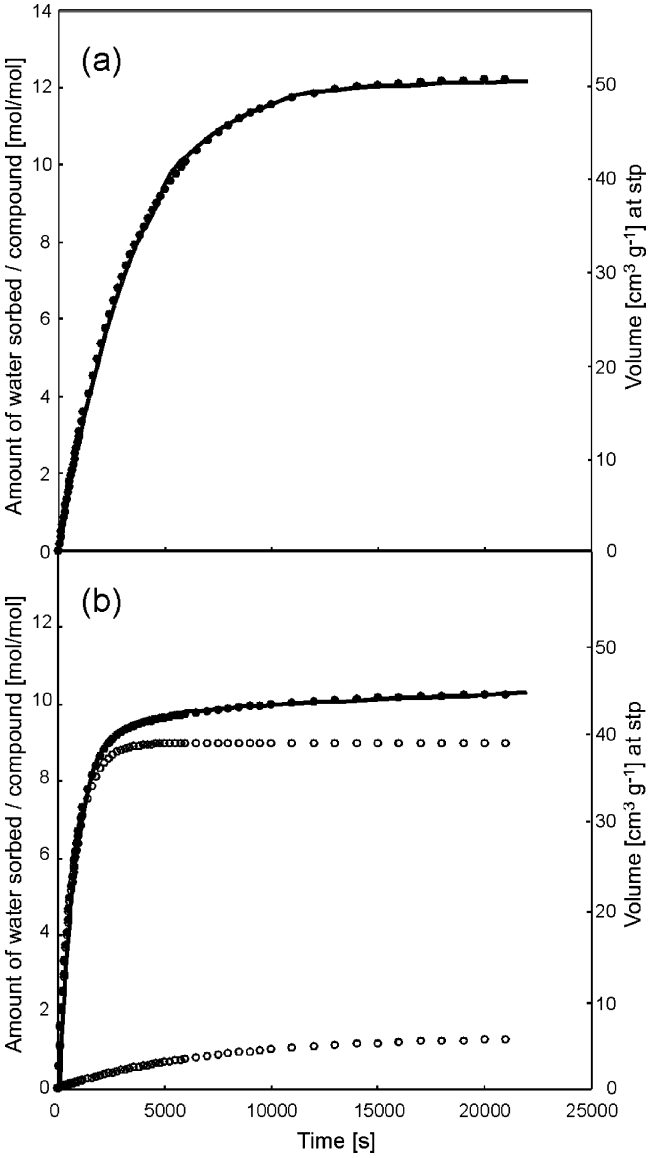

Figure 7. Changes in the amounts of water sorption for **1b** and **3b** at 303 K as a function of time. The vapor pressure is $P/P_0 = 0.7$. (a) The solid line showed the experimental data for **1b**, and solid circles showed the calculated data according to the eq 1. (b) The solid line showed the experimental data for **3b**, and solid circles showed the calculated data according to the eq 2. Open circles showed each of the two components of the calculation.

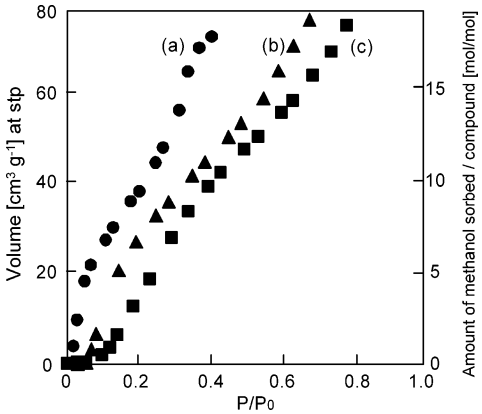

Figure 8. Methanol sorption isotherms of (a) **1b** (●), (b) **2b** (▲), and (c) **3b** (■) at 298 K.

methanol molecule, the methanol sorption probably starts from the low methanol vapor pressures. On the other hand,

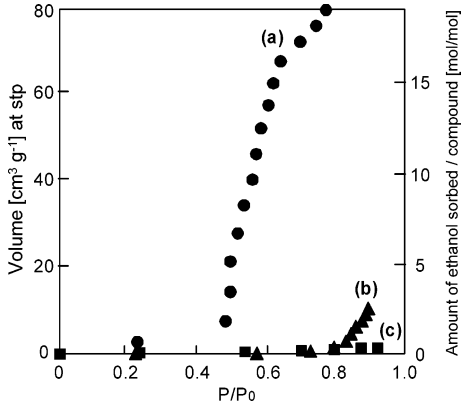

Figure 9. Ethanol sorption isotherms of (a) **1b** (●), (b) **2b** (▲), and (c) **3b** (■) at 298 K.

the sizes of the voids of **2b** and **3b** are smaller than that of the methanol molecule. Therefore, the crystal structures need to change to include the methanol molecules, leading to the existence of the gate pressures. The gate pressure for the methanol sorption of **3b** existed at the higher pressure than that of **2b**, in accordance with the smaller size of the void of **3b**. In the case of the ethanol sorption of **1b**, the gate pressure existed ($P/P_0 = 0.5$). This is probably because the size of the ethanol molecule is much larger than that of the void of **1b**. The compound with the smaller anion charge included larger alcohols, and the difference in the alcohol sorption among **1b**−**3b** is explained by the differences in the void sizes, which decreased with the increase in the anion charges.

Thus, the sizes of the voids, water sorption kinetics, and alcohol sorption properties of **1b**−**3b** systematically changed with the anion charges of the Dawson-type polyoxometalates. These results are the keys to design ionic crystals with novel molecular sieving of polar molecules.

Conclusions

The complexation of Dawson-type polyoxometalates with macrocations formed ionic crystals of $(NH_4)_4[Cr_3O(OOCH)_6(H_2O)_3]_2[\alpha\text{-}P_2W_{18}O_{62}]\cdot 15H_2O$ (**1a**), $(NH_4)_5[Cr_3O(OOCH)_6(H_2O)_3]_2[\alpha_2\text{-}P_2W_{15}V_1O_{62}]\cdot 15H_2O$ (**2a**), and $(NH_4)_7[Cr_3O(OOCH)_6(H_2O)_3]_2[\alpha\text{-}P_2W_{15}V_3O_{62}]\cdot 15H_2O$ (**3a**). The compounds **1a**−**3a** and their guest-free phases **1b**−**3b** showed the honeycomb packing and the symmetry of the constituent ions (i.e., 3-fold symmetry) reflected on the crystal structures. (1) The crystal structures, (2) water sorption kinetics, and (3) alcohol sorption properties of **1b**−**3b** were influenced by the anion charges of the Dawson-type polyoxometalates as follows. (1) The lengths of the *c* axes of **1a**−**3a** and the sizes of the voids of **1b**−**3b** decreased in the order of **1a** ≥ **2a** > **3a** and **1b** > **2b** > **3b**, respectively. In the crystal structures of **1a**−**3a** and **1b**−**3b**, polyoxometalates and macrocations were arranged alternatively along the *c* axes. Therefore, the decrease is probably due to the increase in the anion−cation interaction with the increase in the anion charge. (2) The water sorption profile of **3b** was reproduced

(30) (a) Li, D.; Kaneko, K. *Chem. Phys. Lett.* **2001**, *335*, 50. (b) Uemura, K.; Kitagawa, S.; Fukui, K.; Saito, K. *J. Am. Chem. Soc.* **2004**, *126*, 3817.

by the two components, which were attributable to the diffusion of water molecules in the voids and the expansion in the *c* axis, while that of **1b** was reproduced only by the former component. (3) The compound with the smaller anion charge included larger alcohols, and the difference in the alcohol sorption among **1b**−**3b** was explained by the differences in the sizes of the voids, which decreased with the increase in the anion charges.

Acknowledgment. This work was supported in part by the Core Research for Environmental Science and Technology program of the Japan Science and Technology Agency and Grant-in-Aid for Scientific Research from the Ministry of Education, Culture, Sports, Science, and Technology of Japan.

Supporting Information Available: Figure S1 shows the space-filling model of the arrangements of constituent ions in the *ab* plane of **1b**. Figures S2−S4 show the water sorption isotherms and the calculated water sorption energies for **1b**−**3b**, respectively. X-ray crystallographic file of **1a** in CIF format. This material is available free of charge via the Internet at http:// pubs.acs.org.

CM047879S